Distinct denitrification phenotypes in closely related bacteria: clues to understanding variations in nitrite accumulation among *Stutzerimonas* strains

Martin Menestreau[1], Daniel A. Milligan[1], Louise B. Sennett[1], Linda Bergaust[1], Lars R. Bakken[1], Gary Rowley[2], Morten Kjos[1], James P. Shapleigh[3] and Åsa Frostegård[1]

[1] Faculty of Chemistry, Biotechnology, and Food Sciences, Norwegian University of Life Sciences, Norwegian University of Life Sciences, Ås, Norway

[2] School of Biological Sciences, University of East Anglia, Norwich, United Kingdom

[3] Department of Microbiology, Cornell University, Ithaca, NY, USA

Correspondance: Åsa Frostegård (asa.frostegard@nmbu.no)

Funding: This work was supported by the Research Council of Norway, project no. 325770 (awarded to Å.F.).

Running title: Nitrite accumulation in *Stutzerimonas* strains

Keywords: Denitrification phenotypes, Nitrite accumulation, *Stutzerimonas* strains

Author details:

Martin Menestreau, e-mail: martin.menestreau@nmbu.no; ORCID id: 0000-0001-5060-5903

Daniel A. Milligan, e-mail: daniel.a.milligan@gmail.com; ORCID id: 0009-0002-3792-1308

Louise B. Sennett, e-mail : louise.sennett@nmbu.no; ORCID id: 0000-0001-5445-9712

Linda Bergaust, e-mail: linda.bergaust@nmbu.no; ORCID id: 0000-0001-5100-6611

Lars R. Bakken, e-mail: lars.bakken@nmbu.no; ORCID id: 0000-0002-7293-8108

Gary Rowley, e-mail: g.rowley@uea.ac.uk; ORCID id: 0000-0002-5421-4333

Morten Kjos, e-mail: morten.kjos@nmbu.no; ORCID id: 0000-0003-4448-9082

James P. Shapleigh, e-mail: jps2@cornell.edu; ORCID id: 0000-0002-8628-3966

Åsa Frostegård, e-mail: asa.frostegard@nmbu.no; ORCID id: 0000-0002-4754-5994

Abstract

Nitrite (NO_2^-) is a key denitrification intermediate, formed from nitrate (NO_3^-) and further reduced to nitric oxide (NO), nitrous oxide (N_2O) and dinitrogen (N_2). Transient NO_2^- accumulation is common but varies among bacteria. Despite its potential toxicity and its role in NO and N_2O emissions, the regulatory mechanisms governing NO_2^- accumulation remain poorly understood. We profiled eighteen closely related *Stutzerimonas* strains, including the model *S. perfectomarina* ZoBell, and identified three phenotypic clusters (full, partial and low nitrite accumulators; FNA, PNA and LNA) based on the fraction of NO_3^--N transiently accumulated as NO_2^-. FNA and PNA strains carry both periplasmic (NapA) and membrane-bound (NarG) NO_3^- reductases. FNA strains carry the nitrite reductase NirS clade 1b and NirTB, potentially regulating *nirS*, while PNA strains carry NirS clade 1a and lack NirTB. FNA showed delayed transcription of *nirS* when NO_3^- was present, likely explaining its NO_2^- accumulation phenotype. LNA strains lack *narG* or express it late, balancing NO_2^- production. Addition of NO_3^- halted NO_2^- reduction in FNA but not in others, indicating metabolic control beyond transcription. Our findings reveal diverse NO_2^--handling phenotypes among denitrifiers and provide insights for optimizing wastewater nitrogen removal and soil bioaugmentation strategies to mitigate N_2O emissions.

Introduction

Denitrification is one of the main pathways driving the global nitrogen cycle. Complete denitrification is the four-step reduction of nitrate (NO_3^-) to dinitrogen (N_2) via the intermediate products nitrite (NO_2^-), nitric oxide (NO) and nitrous oxide (N_2O). In this process, the denitrification enzymes Nar, Nir, Nor and Nos are responsible for reduction of NO_3^-, NO_2^-, NO and N_2O, respectively (Zumft 1997). A wide variety of facultative anaerobic organisms, including bacteria, archaea and fungi, can perform all or some of the reduction steps associated with denitrification (Shapleigh 2013; Lycus et al. 2017; Roothans et al. 2025). A shared trait amongst all denitrifiers is that O_2 is the preferred electron acceptor, since it is energetically most favorable. To maintain the physiological processes needed for growth as the O_2 concentration decreases, denitrifiers use a variety of regulatory mechanisms to switch from O_2 to N-oxides as electron acceptors

55 (Spiro 2007; Bakken et al. 2012). Unless the denitrification reductases are synthesized prior to O_2 depletion,
56 their synthesis must take place before the organisms are deprived of energy. If not, they will be unable to
57 produce new proteins needed for coupling respiration to nitrogen oxides (Lycus et al. 2018). These proteins
58 include not only the denitrification enzymes, but also a large set of transcriptional and ancillary factors
59 needed for enzyme production and maturation (Zumft 1997).

60 Current knowledge of how denitrifiers control the transition from aerobic to anaerobic respiration,
61 as well as the onset and coordination of the different denitrification steps, is largely based on studies of a
62 few model organisms capable of complete denitrification of NO_3^- to N_2. These studies have resulted in a
63 relatively clear, though incomplete, understanding of the principal mechanisms involved in the
64 transcriptional regulation of the denitrification genes in these model organisms (Spiro 2012). Several
65 additional, less well-studied control mechanisms, acting at both transcriptional and post-transcriptional
66 levels, have been suggested to influence denitrification phenotypes (Vaccaro et al. 2015; Gaimster et al.
67 2018).

68 The best-studied model denitrifiers *Paracoccus denitrificans*, *Pseudomonas aeruginosa* and
69 *Pseudomonas stutzeri* all transiently accumulate NO_2^- during anaerobic growth on NO_3^-, albeit the
70 accumulated NO_2^- concentrations varies between the species (Carlson and Ingraham 1983). Research
71 extending beyond these well-studied model bacteria has also uncovered significant variations in
72 denitrification phenotypes. A set of new soil isolates representing several bacterial taxa exhibited markedly
73 different levels of NO_2^-, NO and N_2O accumulation (Lycus et al. 2017). Adding further complexity, research
74 has shown that even closely related bacteria can differ significantly in their regulation of denitrification.
75 For example, in a comparison of *Thauera spp*., which are often found in soils and reported as the dominant
76 bacterial genus in wastewater treatment plants (Heider and Fuchs 2015), contrasting phenotypes were
77 observed with respect to the accumulation of denitrification intermediates (Liu et al. 2013). Some *Thauera*
78 strains displayed a rapid and complete onset of all four steps of the denitrification pathway, with little to no
79 accumulation of NO_2^-. A shared feature of these strains was that they carried the periplasmic NapA for
80 dissimilatory NO_3^- reduction but lacked the membrane-bound NarG. In contrast, other strains exhibited a

81 progressive onset of denitrification, reducing all available NO_3^- to NO_2^- prior to any further reduction of
82 NO_2^- , which resulted in NO_2^- accumulation. These NO_2^- accumulating strains carried both NapA and NarG
83 (Liu et al. 2013). All strains induced NO_3^- reduction as O_2 approached depletion, however, the regulatory
84 dynamics varied. While the low NO_2^- accumulating strains initiated transcription of the genes *nirS* and
85 *nosZ*, encoding Nir and Nos at the same time a Nar, the NO_2^- accumulating strains delayed transcription of
86 these genes until all available NO_3^- had been reduced to NO_2^-. This observation led to the tentative
87 suggestion that a NO_3^- responsive mechanism might regulate *nir*-transcription in the NO_2^- accumulating
88 strains, although no direct evidence for this was found.

89 Nitrite is a central molecule in the nitrogen cycle and can be formed and consumed in several redox
90 processes. Under oxic conditions, it is produced from the oxidation of ammonia and can be further oxidized
91 to NO_3^- (nitrification). Under anoxic conditions, NO_2^- is formed through the reduction of NO_3^-. Nitrite
92 reduction is the defining step in denitrification, but NO_2^- is also consumed by processes such as
93 dissimilatory reduction of NO_2^- to NH_4^+ (DNRA) and anaerobic ammonia oxidation (anammox) (Kuypers
94 et al. 2018). Imbalances in the formation and consumption of NO_2^- result in transient accumulation of this
95 compound, which is often undesirable due to its negative impacts on both terrestrial and aquatic
96 environments. Nitrite can be toxic to both eukaryotic and prokaryotic organisms, hampering their growth
97 (Ingram 1973; Bollag and Henninger 1978). Additionally, exogenous NO_2^- can cause increased emissions
98 of the greenhouse gas N_2O through reactions with ferrous iron or organic matter compounds (Van Cleemput
99 and Samater 1996). However, in some systems, NO_2^- accumulation may be desirable. One example is
100 denitratation in wastewater treatment plants, where denitrification is used instead of ammonia oxidation to
101 provide nitrite for the anammox process (Zhuang et al. 2022).

102 In the present study, we examined how transcriptional regulation varies among different strains in
103 the *Stutzerimonas stutzeri* species cluster and how these variations relate to NO_2^- accumulation. We also
104 investigated whether the Crp/Fnr-like regulator DnrE, known to be involved in transcriptional regulation
105 of *S. stutzeri* (formerly *Pseudomonas stutzeri*) (Härtig et al. 1999), affects NO_2^- accumulation in a closely

106 related strain. Moreover, we explored the potential role of sRNAs in determining denitrification phenotypes
107 in these bacteria. sRNAs can act as both activators and repressors of transcription and translation and have
108 been shown to influence the expression of the transcriptional regulator NirR in *P. denitrificans*, thereby
109 indirectly reducing N_2O production (Gaimster et al. 2018; Moeller et al. 2021). Another control mechanism
110 potentially influencing denitrification phenotypes is the competition for electrons between electron
111 pathways to the different denitrification reductases (Cole 2025; Richardson 2025). During both
112 denitrification and aerobic respiration, electrons derived from the TCA cycle are transferred to the
113 quinone/quinol pool in the cell membrane via NADH dehydrogenases (or, in some cases, $FADH_2$
114 dehydrogenases). The quinol pool acts as a key branching point in the electron transport chain. In complete
115 denitrifiers, electrons from the quinol pool are transferred either to dissimilatory NO_3^- reductases –
116 specifically to the periplasmic NapA via NapCB, to the membrane-bound NarG via NarIH, or to both) - or
117 to the bc_1 complex. From the bc_1 complex, electrons are passed to the periplasmic reductases Nir, Nor and
118 NosZ via cytochromes or azurins/pseudoazurins. This step acts as a second branching point in the electron
119 transport chain. Competition for electrons likely occurs not directly between the reductases themselves, but
120 rather at these two branching points (Chen and Strous 2013; Mania et al. 2020). In the present study we
121 specifically investigated whether competition for electrons between NO_3^- and NO_2^- reduction pathways
122 could explain differences in NO_2^- accumulation between the various *S. stutzeri* strains.

123 Despite its importance both in natural and engineered systems, the mechanisms controlling the level
124 of transient NO_2^- accumulation in different denitrifying bacteria remain poorly understood. In this study, we
125 compared the denitrification phenotypes of eighteen closely related bacterial strains within the species
126 cluster formerly known as *Pseudomonas stutzeri*, recently reclassified into the genus *Stutzerimonas*
127 (Lalucat et al. 2022). This genus currently encompasses sixteen species including *S. stutzeri*, which itself is
128 divided into 22 genomovars (Gomila et al. 2022). The *S. stutzeri* complex contains metabolically versatile
129 organisms that are widespread in various environments (Lalucat et al. 2006). The strains we investigated
130 here included the well-studied model organism for denitrification, *S. perfectomarina* strain ZoBell, earlier
131 named *P. stutzeri* (Lehmann and Neumann 1896) or *P. perfectomarina* (ZoBell and Upham 1944). This

132 strain is known to accumulate NO_2^- (Zumft 1997). We also included strains JM300 and AN10, reported to
133 have no or lower NO_2^- accumulation (Wittorf et al. 2018).

134 Our results categorize the eighteen strains into three distinct phenotypic groups based on NO_2^-
135 accumulation. Integrating genome analysis, transcription quantification, and high-resolution denitrification
136 kinetics revealed that differences between NO_2^--accumulating and low accumulating strains primarily
137 involve the presence and regulation of dissimilatory NO_3^- reductases (Nar/Nap). Among the NO_2^--
138 accumulating strains, two subgroups emerged depending on whether all or only part of the supplied NO_3^-
139 was reduced to NO_2^- before further reduction. These subgroups showed consistent differences in their NO_2^-
140 reductases (NirS) in terms of clade affiliation, gene content, and *nirS* gene cluster arrangements. The
141 findings are significant for various biotechnological approaches, such as controlling denitratation in
142 anammox wastewater treatment, and engineering soil microbiomes for N_2O mitigation. Additionally, the
143 results contribute to our understanding of how variations in regulatory phenotypes may influence NO_2^-
144 accumulation across various environments and highlight how organisms optimize energy savings by
145 temporarily blocking steps in the denitrification pathway, albeit simultaneously providing substrates to
146 potentially competing populations.

147 Materials and Methods

148 Strains and growth conditions

149 Eighteen bacterial strains, previously classified as belonging to the *P. stutzeri* species complex (Lalucat et
150 al. 2006; Li et al. 2022), were selected for comparison of their denitrification phenotypes. The strains were
151 obtained from various culture collections. A recent taxonomic revision of the genus *Pseudomonas*
152 reclassified these strains into several species of the novel genus *Stutzerimonas* (Lalucat et al. 2022; Gomila
153 et al. 2022). A list of the strains, including their origin of isolation and culture collection accession numbers,
154 is found in Table S1.

155 All strains were incubated at 20°C in 120 mL serum vials containing 50 mL Sistrom's mineral
156 medium (Sistrom 1960; Bergaust et al. 2010) supplemented with 2 mM KNO_3 or KNO_2, added as filter

157 sterilized solutions. Vials prepared for cultivation under limited O_2 conditions were sealed with gas tight
158 butyl rubber septa and aluminum caps (Matriks AS, Norway), and air was evacuated from the 70 mL
159 headspace by six repetitions of applying vacuum for 360 s and He overpressure for 30 s. The overpressure
160 was released prior to the injection of the desired amount of O_2 and N_2O. Near-equilibrium between
161 headspace and the liquid phase was maintained by vigorous stirring at 600 rpm using a Teflon-coated
162 triangular magnetic bar. The stirring also prevented cell aggregation, ensuring that the cells were evenly
163 dispersed and experienced the intended gas concentrations. At the start of each experiment, the vials were
164 inoculated with 1 mL of aerobically growing bacterial cultures to an initial OD_{600} of 0.05-0.10. The cultures
165 had been raised from frozen stocks and pre-cultured with vigorous stirring under fully oxic conditions for
166 at least 4 generations to minimize the amounts of previously synthesized denitrification enzymes in the
167 cells (Mania et al. 2020; Gao et al. 2021).

168 Gas kinetics and chemical analyses

169 Headspace gases were monitored using a robotized incubation system as described in Molstad et al. (2007)
170 and Molstad et al. (2016). Briefly, gas samples were taken automatically by an autosampler (Agilent GC
171 Sampler 80) through the rubber septa of the vials using a peristaltic pump. The samples were then pumped
172 into a gas chromatograph (Agilent 7890A) for analysis of O_2, N_2O, N_2 and CO_2 and into a
173 chemifluorescence NO analyzer (Model 200A, Advanced Pollution Instrumentation). A thermal
174 conductivity detector was used to measure O_2 and N_2, while an electron capture detector was used to
175 measure N_2O. To maintain a slight overpressure in the vials, each 1 mL gas sample was replaced with a
176 slightly larger volume of He at near-atmospheric pressure. Three replicate vials were measured for each
177 treatment unless otherwise stated (n=3).

178 To determine NO_2^- concentrations, samples were collected from a parallel set of vials to avoid
179 sampling losses and changes in the headspace-to-liquid ratio. The samples were collected manually at
180 regular intervals through the rubber septum using a sterile syringe. Concentrations of NO_2^- were determined
181 immediately after each sampling, using the methodology described in Lim et al. (2018), which is based on

182 the method by Braman and Hendric (1989) and Cox (1980). Briefly, 10 µl liquid sample was injected into
183 a purging device containing a reducing agent (NaI) in 50% acetic acid at room temperature and the NO
184 produced was measured with a chemifluorescence NOx analyzer (Sievers NOA 280i). Samples from three
185 replicate vials were measured (n=3). Calculations based on cubic spline interpolation allowed estimation
186 of values between sampling times.

187 Statistical analyses

188 Statistical analyses were performed using the base statistics software in RStudio. In brief, one-way analysis
189 of variance (ANOVA) tests were performed to assess whether there were significant differences in the
190 levels of denitrification intermediates produced by the different NO_2^- accumulation phenotypes and by the
191 various overexpression mutants. When differences occurred ($p = 0.05$), mean pairwise comparisons were
192 performed using Tukey's test (HSD) for the post hoc analysis of the ANOVA models. Normality was tested
193 using homoscedasticity plots and the Shapiro-Wilks test of the residuals ($p > 0.05$).

194 Transcription analysis

195 Samples for RNA extraction (approximately 5 x 10^8 cells per sample) were taken at intervals from the liquid
196 phase. Cells were pelleted at 10,000 g for 7 minutes at 4°C and stabilized using RNAprotect (Bacteria
197 Reagent, Qiagen) according to the manufacturer's protocol. Total RNA was extracted using the RNeasy
198 Mini Kit (Quiagen). RNA concentrations were measured using the Qubit RNA BR Assay Kit (Life
199 Technologies). Genomic DNA was removed with Turbo DNase (Life Technologies) and genomic DNA
200 contamination was ruled out by SYBR green qPCR amplification using primers for *nosZ* (Table S2) prior
201 to reverse transcription. The assays were run on an Applied Biosystems StepOnePlus system, and samples
202 with values < 5 *nosZ* copies per reaction were deemed gDNA free (Lim et al. 2016). Reverse transcription
203 was then carried out with Maxima First Strand cDNA Synthesis Kit (Thermo Scientific), the product was
204 diluted, and gene transcripts were quantified by digital droplet PCR (ddPCR) using EvaGreen on a qx200
205 Droplet Generator and Reader, Applied Biosystems 2720 Thermal Cycler. All primers used are listed in
206 Table S2.

207 ## Deletion of *narG* and *dnrE* in *Stutzerimonas decontaminans* strain 19SMN4

208 The pACRISPR/pCasPA system developed by Chen et al. (2018) for genome editing in various
209 *Pseudomonas* species was used to construct the two deletion mutants, Δ*narG* and Δ*dnrE*, in *Stutzerimonas*
210 *decontaminans* 19SMN4. pACRISPR plasmids specific to the targeted gene were constructed to contain a
211 spacer targeting the specific gene designed using the tool CRISPOR (Concordet and Haeussler 2018) and
212 a repair template consisting of 1000-bp flanking sequences, upstream and the downstream of the gene. The
213 pCasPA was electroporated into *S. decontaminans* strain 19SMN4 following the protocol of Choi et al.
214 (2006), but with electroporation parameters optimized for this strain (2500V, 200Ω, 25µF, 2 mm cuvette).
215 Colonies containing pCasPA were selected after incubation on LB agar in the presence of 50 µg mL^{-1}
216 tetracycline. Before the second electroporation for introduction of the gene specific plasmid pACRISPR,
217 the strain containing the pCasPA plasmid was induced for 2 hours with 2 mg mL^{-1} L-arabinose, followed
218 by electroporation under the same conditions as the first electroporation. Transformants were then selected
219 on 50 µg mL^{-1} tetracycline and 150 µg mL^{-1} carbenicillin plates. The deletions were validated by PCR (for
220 primers see Table S2) and Sanger sequencing. Plasmids were then cured with 10% w/v sucrose in
221 successfully mutated cells.

222 ## *Stutzerimonas perfectomarina* ZoBell sRNA overexpression mutants

223 Small RNAs (sRNAs) were overexpressed in *Stutzerimonas perfectomarina* ZoBell using the arabinose-
224 inducible vector pL2020 (Sommer et al. 2017). The pL2020 plasmid was linearized by digestion with NdeI
225 and HindIII. sRNAs were amplified from *S. perfectomarina* ZoBell genomic DNA using overlapping PCR.
226 The resulting PCR fragments were assembled with the digested vector using the NEBuilder HiFi DNA
227 Assembly Master Mix (New England Biolabs) and transformed into *E. coli* DH5α competent cells.
228 Transformants were selected on LB agar plates containing 30 µg mL^{-1} chloramphenicol. Positive clones
229 were screened by colony PCR and verified by Sanger sequencing. Constructed plasmids were subsequently
230 electroporated into the *S. perfectomarina* ZoBell host strain using an adapted protocol (Choi et al. 2006)
231 with optimized electroporation parameters as described above. The growth of the sRNA overexpression

232 mutants was assessed in LB medium supplemented with 30 µg mL^{-1} chloramphenicol to maintain plasmid
233 selection.

234 Genome sequencing and assembly

235 DNA was extracted with the QIAmp DNA Mini Kit (Qiagen, USA) and sent to the Norwegian Sequencing
236 Centre (University of Oslo) for TruSeq Nano preparation and Illumina MiSeq sequencing. Reads were
237 trimmed using Nesoni clip (https://github.com/Victorian-Bioinformatics-Consortium/nesoni) and contigs
238 were assembled using Velvet (Zerbino and Birney 2008). Sequence annotation was carried out on the RAST
239 server (Aziz et al. 2008). NCBI accession numbers are listed in Table S1.

240 Gene sequence analyses and phylogenetic determinations

241 Sequences coding for housekeeping genes assigned to strains in the *P. stutzeri* species complex, as well as
242 regulatory and structural genes encoding relevant nitrogen cycle processes, were retrieved from the NCBI
243 databases. For protein-coding genes, the match sequences that represented uninterrupted open reading
244 frames (ORFs) were identified, and gene synteny was compared for strains for which extensive operon data
245 was available. The phylogenetic relationship of the strains was determined based on a multilocus sequence
246 analysis (MLSA) of the genes encoding the small subunit RNA (16S rRNA), gyrase B (*gyrB*) and RNA
247 polymerase (*rpoD*). The sequences were complete, except in the case of 16S rRNA genes where the first
248 30 residues were omitted, as they were not available for strain DSM 50238. Genes were aligned using
249 MUSCLE v. 3.8.31 (Edgar 2004) and examined before Jukes Cantor distance estimation and maximum-
250 likelihood tree construction, using PhyMl 3.1 (Guindon et al. 2010). Amino acid-based enzyme phylogenies
251 were calculated using Clustal Omega (Sievers et al. 2011) and phylogenetic trees were constructed using
252 the Whelan and Goldman model in PhyMl.

253 Results

254 Nitrite accumulation phenotypes and phylogeny

255 Analyses of the denitrification phenotypes revealed significant differences in transient NO_2^- accumulation
256 among the strains (Table 1). When incubated under denitrifying conditions with initially 100 µmol $vial^{-1}$ of

257 NO_3^- (2 mM), the full nitrite accumulator (FNA) strains reduced ≥89 % of the provided NO_3^- to NO_2^- before
258 any NO_2^- reduction took place (Figure 1a and Figure S1). The partial nitrite accumulator (PNA) strains
259 (Figure 1b and Figure S2) exhibited transient NO_2^- accumulation, amounting to about half of the provided
260 NO_3^- (43.7- 62.2 µmol vial^{-1} of NO_2^-). The low nitrite accumulator (LNA) phenotype (Figure 1c and Figure
261 S3) showed no or little NO_2^- accumulation (0.2-1.6 µmol vial^{-1}), except for strains 24a75 and 4C29, which
262 transiently accumulated 11.3 and 17.1 µmol NO_2^- vial^{-1}, respectively.

263 A phylogenetic tree was constructed, incorporating the eighteen *Stutzerimonas* strains selected for
264 analysis of denitrification phenotypes, along with additional related strains. Each strain´s classification is
265 marked in the phylogenetic tree with red (FNA), yellow (PNA) or blue (LNA) (Figure 2). The tree was
266 based on multilocus sequence analysis (MLSA) of two complete housekeeping genes (*gyrB* and *rpoD*) and
267 nearly complete 16S rRNA gene sequences. Only limited congruence was observed between phylogeny
268 and the NO_2^- accumulation phenotype: FNA and PNA strains clustered together and were often intertwined,
269 whereas LNA strains were distributed across multiple, widely separated branches. The neighbor joining
270 tree based on kmer clustering of a more extensive collection of genomes from *Stutzerimonas* strains (Figure
271 S4) revealed a similar pattern, also consistent with other recently published phylogenetic studies (Li et al.
272 2022; Gomila et al. 2022).

273 Selected genetic features related to denitrification

274 An analysis of denitrification related gene clusters was performed to identify possible relationships with
275 the NO_2^- accumulation phenotypes (Table 1). All eighteen strains carry the *napEDABC* gene cluster
276 encoding periplasmic nitrate reductase (Nap). Nap also was the dominant NO_3^- reductase in the clustered
277 set of genomes (Figure S4). Two strains in the LNA group (DNSP21 and 28a3) rely only on Nap for
278 dissimilatory NO_3^- reduction, since they lack the cytoplasmic nitrate reductase Nar, encoded by the *nar*
279 genes. The *narGHJIKMXL* cluster was found in all other strains. A notable difference in *nar*-related genes
280 among the phenotype groups was the presence of the *dnrE* gene, which was found in all FNA and PNA
281 strains but was absent in all LNA strains. DnrE is located within the *nar* gene cluster, downstream of *narXL*,

282 which encodes a two-component regulatory system that senses NO_3^- and NO_2^- under anaerobic conditions
283 (Härtig et al. 1999). DnrE belongs to the DNR group (dissimilatory nitrate respiration regulators), a
284 subgroup of transcriptional regulators related to the Fnr/Crp family (Trunk et al. 2010; Ebert et al. 2017).
285 However, the precise physiological function of DnrE has not yet been fully elucidated.

286 All analyzed strains carried the *nirS* gene encoding the cytochrome cd_1 nitrite reductase (Zumft
287 1997). The *nirS* gene is part of a large gene cluster encoding various enzymes involved in the synthesis and
288 function of NirS (Jüngst et al. 1991; Philippot 2002). The FNA and PNA strains have identical *nirS* gene
289 cluster configurations, apart from the presence of *nirTB* in the FNA strains, while the *nirS* gene cluster in
290 the LNA strains is more diverse (Figure S5). Based on their amino acid sequences, the NirS reductases
291 have been divided into several clades. (Jones et al. 2008; Pold et al. 2024). Following this classification,
292 the NirS type of the FNA organisms in the present study belongs to clade 1b, while that of the PNA and
293 LNA strains belong to clade 1a (Table 1), except the LNA strain JM300 which carries the NirS clade 1b
294 (Figure S5). A common trait for all analyzed (Table 1) or clustered (Figure S4) *Stutzerimonas* strains with
295 clade 1b NirS is the consistent presence of the genes *nirT* and *nirB*. NirT and NirB are tetraheme and diheme
296 cytochromes, respectively, with a putative role in electron transfer and possibly also in the catalytic
297 activation of the cd_1 cytochrome (Härtig and Zumft 1999; Zajicek et al. 2004). The *nirTB* genes are absent
298 in all clade 1a strains.

299 Seven of the analyzed strains carried the gene *nirK*, encoding the copper-containing nitrite
300 reductase NirK, in addition to *nirS*. Of the 314 genomes in the clustered tree, 111 had the *nirK* gene (Figure
301 S4). The *nirK* genes were found in strains across all three NO_2^- accumulator groups (Table 1). Previously,
302 *nirK* was divided into two main clades based on copper-binding histidine motifs: TRPHL for clade I and
303 SSFH(V/I/P) for clade II (Jones et al. 2008; Declayre et al. 2016). A recent study (Pold et al. 2024) proposed
304 a more detailed classification, reassigning *Stutzerimonas* strains with clade I NirK to clade 1a, and those
305 with clade II to clade 1e. In the analyzed *Stutzerimonas* strains carrying the *nirK* clade I gene (1a), the gene
306 is consistently followed by *nirV*. This was observed in two of the strains in the present study, both belonging

307 to the LNA phenotype group (Table 1). Half of the FNA strains analyzed in this study, along with one PNA
308 strain, possess *nirK* clade II (1e), consistently followed by the *norCBQD* gene cluster.

309 The nitric oxide reductase cNor, which was present in all eighteen strains, is encoded by the
310 *norCBD* operon located in the denitrification island together with the *nir* and *nos* clusters (Zumft 1997;
311 Vollack et al. 1998). The *norCBQD* cluster present downstream of the *nirK* gene likely encodes a
312 supplementary cytochrome *c*-dependent nitric oxide reductase (cNor), which can provide an alternative or
313 redundant NO reduction pathway. The gene cluster *nosRZDFYL* encoding the nitrous oxide reductase
314 (NosZ) clade I was also found in the denitrification island in all the studied *Stutzerimonas* strains. The *nor*
315 and *nos* gene cluster arrangements were identical in all strains (Table 1).

316 Denitrification kinetics and transcription analysis

317 Electron flow rates to the different reductases were calculated from denitrification kinetics measured for all
318 eighteen strains during and after the switch from aerobic respiration to denitrification when incubated with
319 1% initial O_2 and 2 mM NO_3^- (100 µmol vial^{-1}). All strains could perform the complete denitrification
320 process, reducing NO_3^- to N_2. Examples for some representative strains are shown in Figure 1 and Figure
321 3, while Figure S1 and Figure 3 show the denitrification kinetics for the remainder. Common to all strains,
322 irrespective of which NO_2^- accumulation group they belonged to, was that NO_3^- reduction started when the
323 O_2 had decreased to 10-15 µmol vial^{-1} (corresponding to 0.6-0.9 µM in the liquid). The FNA strains reduced
324 all the provided NO_3^- to NO_2^- before any NO_2^- reduction took place, as shown by the lack of intermediate
325 gas products (Figure 1a and Figure S1). The start of NO_2^- reduction coincided with the peak of NO_2^-
326 accumulation and was accompanied by nearly simultaneous production of NO, N_2O and N_2. The sequential
327 reduction of NO_3^- and NO_2^- in the FNA strains is also reflected in the electron flow kinetics (Figure 1d and
328 Figure S1), with nearly no overlap between the curve showing the electron flow rate to NO_3^- ($V_{eNar/Nap}$, red
329 shading) and that to NO_2^- (V_{eNir}; purple shading) and a clear separation between O_2 reduction (V_{eO2}; blue
330 shading) and NO_2^- reduction (V_{eNir}; purple shading). The electron flow for the FNA strains typically showed
331 a prominent dip when the cultures shifted from NO_3^- reduction to NO_2^- reduction (Figure 1d, Figure 3e and

332 Figure S2), suggesting that only a fraction of the cells respired NO_2^- as found for *Paracoccus denitrificans*
333 (Lycus et al. 2018).

334 The PNA and LNA strains reduced NO_3^- and NO_2^- simultaneously, as indicated by the production
335 of NO and N_2O, followed by the appearance of N_2 (Figure 1b-c, Figure S2 and Figure S3). The strains
336 CCUG 11256 (PNA) and 28a3 (LNA) were similar in their denitrification phenotypes (Figure 1b-c), except
337 for the transient accumulation of NO_2^- by the PNA strain. The simultaneous reduction of NO_3^- and NO_2^-
338 was reflected in the overlap between the areas under the curves for $V_{eNar/Nap}$ (red shading) and V_{eNir} (purple
339 shading) (Figure 2e-f, Figure S2 and Figure S3). Production of N_2 was detected somewhat later, when O_2
340 was near depletion. For both the PNA and LNA groups, the electron flow indicated smooth transitions
341 between the different electron acceptors with no distinct dips and thus an overlap between the curves for
342 $V_{eNar/Nap}$ and Ve_{Nir}.

343 All three NO_2^- accumulation phenotypes showed little transient accumulation of NO and N_2O
344 (Table 1), suggesting a strong regulatory control of the production and consumption of these gaseous
345 denitrification intermediates. When incubated with 1% initial O_2 and 2 mM initial concentration of NO_3^-,
346 the maximum net NO production was 9.1–70.5 nmol vial^{-1} with no significant (p = 0.598) difference
347 between the phenotype groups in terms of maximum NO accumulation. The N_2O accumulation remained
348 low for all strains, ranging between 0.3 and 89 nmol vial^{-1}, and was significantly lower for FNA compared
349 to LNA (p = 0.030), while PNA exhibited intermediate levels, showing no significant difference from either
350 FNA or LNA (p = 0.840 and 0.217).

351 Transcription of the denitrification reductase genes *narG, napA*, *nirS*, *norB* and *nosZ* was monitored
352 in the strains ZoBell (FNA) and JM300 (LNA) during and after the transition from aerobic respiration to
353 denitrification, along with the denitrification kinetics (Figure 3). In addition, transcription of the *nirK* gene,
354 which is lacking in strain ZoBell (Table 1), was monitored in strain JM300. Strain ZoBell reduced all NO_3^-
355 (100 µmol vial^{-1}) to NO_2^- before any significant NO_2^- reduction took place (Figure 3a), confirming its
356 classification into the FNA group. This was also reflected in the electron flow kinetics which showed that

electrons were channeled to Nir only once the electron flow to Nar stalled due to NO_3^- depletion (Figure 3e). Transcription of *napA* and *nosZ* in strain ZoBell (Figure 3c) was detected already at 0 h post inoculation (hpi). Increased transcription was observed for all the monitored genes at 10-13 hpi when less than 10 µmol of O_2 remained in the vial, with an initial transcription peak for most genes at 18 hpi. Although transcripts for genes involved in all four denitrification steps were detected during this initial peak, it resulted in only minimal reduction activity, except for NO_3^- reduction. A second pulse of transcription occurred once all NO_3^- had been reduced and the NO_2^- concentration reached its maximum. During this second event, the maximal levels of *norB* and *nirS* (inset) transcription were observed at 30-35 hpi. There was also a notable increase in *nosZ* transcription, although not surpassing what was measured in the initial phase. These peaks corresponded to the nearly simultaneous reduction of NO_2^-, NO and N_2O (Figure 3a). Transcription was sustained until all intermediates were fully reduced to N_2.

The LNA strain JM300 (Figure 3b, d, f) reduced NO_3^- to gases, via NO_2^-, without any detectable net accumulation of NO_2^-. NO and N_2O became detectable when the O_2 concentration was approximately 20 µmol vial^{-1}, corresponding to1.2 µM in the liquid (at 7.5 hpi). Concentrations of these gases peaked around 11 hpi, immediately followed by N_2 production. The simultaneous reduction of the different electron acceptors is seen in the gradual increase in total electron flow rates in JM300 as well as in the other LNA strains (Figure 3f and Figure S3). Also notable is the absence of the significant dip in the electron flow rates that was observed in most of the FNA strains during the shift from NO_3^- to NO_2^- reduction (Figure 3e and Figure S1).The overlapping $V_{eNar/Nap}$ and V_{eNir} curves (Figure 3f) reflect the simultaneous reduction of NO_3^- and NO_2^-, similar to the other strains characterized as LNA (Figure 2c, f and Figure S3). An important observation was that the transcription of *narG* had a five-hour delay compared to the other genes, meaning that NO_3^- reduction was carried out by the periplasmic nitrate reductase Nap during the early phase of denitrification. A small delay was also observed for *nirS*, *nirK*, and *norB* transcription compared to *napA* and *nosZ* transcription. A delayed *narG* transcription was also observed in the LNA strain DSM 50238 (Figure S6). This strain exhibited a similar transcriptional profile as JM300, although it lacks *nirK*.

382 ## Effect of *narG* and *dnrE* deletions on nitrite accumulation

383 The wild-type PNA strain 19SMN4 carries *narG*, which is either absent (Table 1) or transcribed with a
384 delay (Figure 3 and Figure S6) in the LNA strains, as well as *dnrE*, which is absent in all the LNA strains
385 (Table 1). We hypothesized that deletion of either gene would shift strain 19SMN4 from the PNA to the
386 LNA phenotype. Specifically, we predicted that NO_3^- reduction rate would slow down in the *narG* mutant,
387 as it would rely solely on the periplasmic NO_3^- reductase Nap for dissimilatory NO_3^- reduction, resulting in
388 reduced NO_2^- accumulation. Furthermore, given that all LNA strains lack the *dnrE* gene (Table 1), we
389 hypothesized that the absence of this transcriptional regulator would reduce or delay the transcription of
390 *narG* in the presence of NO_3^-, compared to the wild-type. This would similarly result in reduced NO_2^-
391 accumulation producing a phenotype resembling that of the LNA strains. To test these hypotheses, we
392 generated deletion *narG* and *dnrE* mutants in the PNA strain 19SMN4.

393 A comparison of the denitrification phenotypes of the wild-type and the two mutants showed that
394 the mutants remained complete denitrifiers, as all provided NO_3^- was fully reduced to N_2 (Figure 4). Both
395 the wild-type and the mutants transitioned to denitrification, indicated by the accumulation of low amounts
396 of NO (16.5-43.2 nmol vial^{-1}) and N_2O (11.0-34.9 nmol vial^{-1}), when O_2 fell below 7.5 µmol vial^{-1}(0.45 µM
397 in the liquid). The two mutants and the wild-type strain showed, however, different denitrification
398 phenotypes regarding their NO_2^- accumulation and the time it took to complete denitrification (seen as an
399 N_2 plateau). The wild-type strain accumulated approximately 50% of the provided 100 µmol NO_3^- vial^{-1} as
400 NO_2^- (62.8 µmol vial^{-1}), supporting its classification as PNA, determined in a separate experiment (Figure
401 S2) where this strain accumulated 44.0 µmol vial^{-1} NO_2^- . In contrast to the wild-type, the Δ*narG* mutant
402 accumulated <1.3 µmol vial^{-1} NO_2^- (Figure 4). It had thus obtained an LNA phenotype similar to the strains
403 *Stutzerimonas frequens* DNSP21 and *S. stutzeri* 28a3 (Figure 1c and Figure S3a), both of which lack *narG*
404 and thus use only Nap for dissimilatory NO_3^- reduction (Table 1). Moreover, and as expected, deleting *narG*
405 slowed denitrification so that the reduction of the provided NO_3^- to N_2 took almost three times longer than
406 for the wild-type (78 h *vs* 28 h). Knocking out the *dnrE* gene had a less severe effect on the time it took to

407 complete denitrification (38 h). However, and contrary to our expectations, the Δ*dnrE* mutant showed
408 increased accumulation of NO_2^- compared to the wild-type, reaching 80.1 ± 4.99 µmol vial^{-1}.

409 Competition for electrons between the NO_3^- and NO_2^- reduction pathways

410 To investigate whether competition for electrons between the NO_3^- and NO_2^- reduction pathways
411 influences NO_2^- accumulation, we added NO_3^- to actively NO_2^- reducing cultures, three strains were studied
412 (ZoBell, FNA; 19SMNA, PNA and JM300, LNA), representing each of the phenotype groups (Figure 5a-
413 c). The cultures were initially incubated under the denitrifying conditions described above to induce the
414 development of the denitrification proteome, after which the cells were transferred to new anoxic vials
415 (initial OD_{600} 0.3) with medium containing 100 µmol NO_2^- vial^{-1} (corresponding to 2 mM NO_2^- in the
416 medium) (t=0). When approximately one third of the initial NO_2^- had been reduced, 100 µmol vial^{-1} of NO_3^-
417 (corresponding to 2 mM NO_3^- in the medium) was added to the vial. For strain ZoBell (Figure 5a), the
418 addition of NO_3^- to the actively NO_2^- respiring culture led to an immediate shift to NO_3^- respiration and a
419 complete halt of the NO_2^- reduction until all the added NO_3^- had been reduced. This shift is also seen from
420 the plummeting of the NO concentration and the plateauing of N_2. Once all the NO_3^- had been reduced,
421 NO_2^- respiration resumed along with the downstream denitrification steps as seen from the decrease of NO_2^-
422 and the concomitant accumulation of NO (<50 nmol vial^{-1}). N_2 increased until it reached a plateau at
423 approximately 200 µmol N_2-N vial^{-1}, reflecting the complete reduction of the added NO_3^- and NO_2^-.

424 In a similar experiment, strain 19SMN4 (PNA) was observed to reduce NO_3^- and NO_2^-
425 simultaneously, and continuously reduced NO_2^- further to N_2, as seen by the constant increase of N_2 and
426 lack of an intermittent N_2 plateau (Figure 5b). NO_3^- was apparently reduced faster than NO_2^-, resulting in a
427 transient accumulation of NO_2^- from 75 to 123 µmol vial^{-1}(thus about half of the added NO_3^-) until all the
428 available NO_3^- was depleted. The LNA strain JM300 (Figure 5c) continued to reduce NO_2^- despite the
429 addition of NO_3^-, with no accumulation of NO_2^-. The NO_2^- reduction proceeded without any apparent
430 reduction in rate until all NO_3^- and NO_2^- had been consumed, seen as N_2-N reaching a plateau. As observed

431 with strain ZoBell, the accumulation of NO peaked at ≤ 50 nmol vial^{-1} in experiments with strains 19SMN4
432 or JM300 (Figure 5b-c).

433 As previously stated, the quinol pool serves as the branching point where electrons are either
434 transferred toward NO_3^- reduction via the Nar and Nap pathways or toward the bc_1 complex to feed Nir,
435 Nor, and Nos. The apparent blocking of NirS activity observed in denitrifying FNA cells (strain ZoBell)
436 that received NO_3^- (Figure 5) could theoretically result from restricted electron flow either to bc_1, or from
437 bc_1 to Nir via cytochromes. To test whether Nir activity could resume when electrons were provided directly
438 to cytochrome c, we added TMPD and ascorbate along with NO_3^- to denitrifying cells. TMPD (N, N, N′,
439 N′-tetramethyl-p-phenylenediamine) is an artificial electron donor. It supplies an excess of electrons to
440 cytochrome *c*, which are passed on to Nir, Nor, and Nos. We expected this to alleviate the inhibition of
441 NO_2^- reduction. However, TMPD only marginally enhanced Nir activity (Figure 5d-e). After NO_3^- addition,
442 cultures with TMPD (Figure 5e) accumulated 111.0 ± 1.9 µmol NO_2^- vial^{-1}, corresponding to 88.8% of the
443 provided NO_3^- (125 µmol vial^{-1}). Control vials receiving only NO_3^- (Figure 5d) accumulated 121.9 ± 6.3
444 µmol NO_2^- vial^{-1} (100%), suggesting a partial rerouting of the electron flow toward Nir also seen from the
445 tripling of NO accumulation in cultures treated with TMPD (46.8 vs. 151.7 nmol vial^{-1}). This interpretation
446 is supported by an increased N_2 accumulation rate (1.9 µmol N vial^{-1} h^{-1}) during NO_2^- accumulation with
447 TMPD, compared to nearly zero in the control (0.06 µmol N vial^{-1} h^{-1}). Together, these results strongly
448 suggest that NO_3^- inhibits NirS activity by restricting electron transfer from bc_1 to NirS (via cytochromes)
449 rather than by limiting the electron flow to bc_1. Surprisingly, no significant increase in Nor or Nos activity
450 was observed with TMPD.

451 Analysis of a possible role of sRNAs in regulating nitrite accumulation

452 We investigated potential regulatory mechanisms underlying the nitrite accumulation phenotype by
453 examining the role of small RNAs (sRNAs). Inclusion of selected sRNAs was based on their previous
454 association to either regulation of the broader nitrogen cycle, to denitrification specifically, to anaerobic
455 regulators, and to regulators located within denitrification gene clusters in *Stutzerimonas* sp. (Lin et al.

456 2015; Zhan et al. 2016; Wang et al. 2022). With these criteria, eight putative sRNAs (crcZ, nfiS, P11, P15,
457 pda200, phrS, prrF1, rsmY) were selected for investigation and overexpression strains constructed.
458 Overexpression has been used to assign function to sRNAs from a wide range of bacterial species and
459 associated processes (Massé and Gottesman 2002; Gaimster et al. 2019). We assessed the NO_2^-
460 accumulation under anaerobic conditions for the sRNA-overexpressing strains (Figure S8). During
461 anaerobic growth, NO_2^- accumulation peaked between 83.2 ± 7.7 and 104.2 ± 0.4 μmol vial^{-1}. However,
462 pairwise Tukey HSD tests revealed no statistically significant differences in NO_2^- accumulation between
463 any of the overexpression strains and the control ($p > 0.05$).

464 Discussion

465 During denitrification, intermediate products, such as NO_2^-, are released from the bacteria into the
466 environment, forcing the cells that produce them to compete with nearby microbes for these electron
467 acceptors. Nitrite accumulation can have severe environmental consequences, as it plays a central role in
468 the emissions of N_2O, NO and HONO from various environments (Bhattarai et al. 2018; Frostegård et al.
469 2022; Song et al. 2023) and can also hamper N removal efficiency in wastewater plants (Zhou et al. 2011).
470 Despite this, the mechanisms that determine the levels of NO_2^- produced by various denitrifying bacteria
471 have received relatively little attention and remain poorly understood. Likewise, there is scarcity of studies
472 on the extent to which NO_2^- accumulation varies among closely related organisms. Our study revealed a
473 greater diversity in denitrification phenotypes within the genus *Stutzerimonas* than previously recognized,
474 with strains exhibiting full, partial, or low NO_2^--accumulating phenotypes. Based on gene surveys,
475 transcriptional and mutational analyses, and phenotype determinations, we have identified multiple factors
476 contributing to intermediate NO_2^- accumulation in *Stutzerimonas* strains. These factors include genetic
477 configurations as well as regulatory mechanisms operating at both the transcriptional and post-
478 transcriptional/metabolic levels.

479 Among the eighteen closely related strains in the *Stutzerimonas* genus, eight were classified as full
480 NO_2^- accumulators (FNA), including the denitrification model organism *S. perfectomarina* strain ZoBell,

481 known to accumulate NO_2^- (Zumft 1997). Three strains were classified as PNA, among them strain AN10,
482 also reported earlier to accumulate modest levels of NO_2^- (Wittorf et al. 2018), while seven strains were
483 low NO_2^- accumulators (LNA), including strain JM300, consistent with previous findings for this strain
484 (Wittorf et al. 2018). The phenotype grouping showed partial congruence with phylogeny (Figure 2). Strains
485 classified as FNA and PNA were phylogenetically intertwined, and in a couple of cases, even strains of the
486 same species belonged to different phenotype groups. The LNA strains were phylogenetically separated
487 from the two other phenotype groups with one exception (DNSP21). The tree produced from *Stutzerimonas*
488 genome clustering supported these observations, except that strains DNSP21 and 24a75 showed proximity
489 (Figure S4). The limited congruence between phylogeny or genome clustering and NO_2^- accumulation
490 phenotype aligns with findings from the genus *Thauera* (Liu et al. 2013) and underscores the need for
491 caution against inferring regulatory phenotypes based solely on taxonomic relatedness.

492 The genome survey of denitrification-related genes (Table 1) provided some indications of
493 differences that might influence NO_2^- accumulation. However, the gene content did not conclusively explain
494 the three phenotype groups. Variations were found in the gene clusters encoding both dissimilatory nitrate
495 and nitrite reduction, whereas the clusters for NO and N_2O reduction had consistent gene arrangements
496 across all three groups. A previous investigation of *Thauera* strains (Liu et al. 2013) suggested that the type
497 of dissimilatory NO_3^- reductases play a key role since the NO_2^- accumulating strains carried both the *nar*
498 and *nap* clusters, while the strains that did not accumulate NO_2^- had only the *nap* cluster. In the present
499 study of *Stutzerimonas* strains, the genome survey (Table 1) revealed that all FNA and PNA strains carried
500 the *nar* genes. However, unlike the *Thauera* strains, the *nar* cluster was also found in all but two of the
501 LNA strains, indicating that the presence of *narG* cannot reliably predict NO_2^- accumulation.

502 To investigate whether transcriptional control could explain why organisms with the same genotype
503 displayed contrasting phenotypes, we measured transcriptional activity of denitrification reductases in LNA
504 strains. Strain JM300 showed significantly delayed *narG* transcription by ~4-6 h compared to the other
505 denitrification related genes (Figure 3d), implying that it relied only on Nap for NO_3^- reduction in the
506 interim. These results suggest that the LNA phenotype arises when bacteria either lack *nar* on the genome

507 or have delayed transcription of *nar*. Here the sole reliance on Nap results in slower NO_3^- reduction and
508 allows Nir to maintain pace. Interestingly, the JM300 strain carries the NO_2^- reductase gene *nirK* in addition
509 to *nirS*, and it cannot be excluded that this was a factor determining the lack of NO_2^- accumulation. To
510 explore this, we performed a real-time PCR-based transcription analysis of the LNA strain DSM 50238,
511 which carries both *napA* and *narG* but only has *nirS* for dissimilatory NO_2^- reduction (thus lacking *nirK*).
512 Although copy numbers were lower than those from the ddPCR analysis, the temporal pattern of
513 transcription was the same as JM300 and also showed a significant delay in *narG* transcription (Figure S5).
514 Collectively this reinforces role of NarG as a primary factor in determining whether a denitrifier
515 accumulates NO_2^-. This is further supported by the results from the *narG* knock-out mutant, which shifts
516 PNA strain 19SMN4 to a LNA phenotype (Figure 4). While the presence and activity of Nar appear to be
517 significant factors in determining whether a strain accumulates NO_2^-, they do not conclusively explain the
518 difference between the phenotype groups. A primary distinction between the FNA group and the PNA/LNA
519 groups appears to lie in their transcriptional control of *nirS* (Figure 3). The FNA phenotype was
520 characterized by a progressive onset of denitrification, whereas the LNA phenotype showed a rapid and
521 complete onset, similar to reports on *Thauera* strains (Liu et al. 2013). In that study, the FNA strain *Thauera*
522 *terpenica* showed a low transcription peak of *nirS* shortly before O_2 depletion, but the main transcription
523 was delayed and coincided with the peak of NO_2^- accumulation and depletion of NO_3^-. This precise timing
524 of *nirS* transcription led to the tentative suggestion that NO_3^- interacted with one of the regulatory proteins
525 involved in *nirS* transcription, possibly a repressor protein, though no evidence was provided to support
526 such a mechanism. The present, more detailed analysis revealed a similar transcription pattern in *S.*
527 *perfectomarina* strain ZoBell. Taken together, the findings suggest that temporal control of transcription
528 plays a major role in the near complete NO_2^- accumulation in FNA strains, although other control
529 mechanisms are likely at play as well.

530 The FNA strains showed a nearly complete blockage of NO_2^- reduction while NO_3^- was present,
531 whereas the PNA strains reduced NO_2^- in the presence of NO_3^-, albeit not at a sufficiently high rate to
532 immediately reduce the produced NO_2^- as effectively as the LNA strains (Figure 5a-c). This suggests

533 simultaneous electron flow to Nar/Nap and Nir, allowing some Nir activity in the presence of NO_3^- for PNA
534 and LNA organisms. For FNA organisms it seems unlikely that Nar outcompetes the bc_1 complex for
535 electrons significantly more than in PNA strains. One notable difference could be the clade of NirS,
536 classified as clade 1b in the FNA strains and clade 1a in the PNA strains. This distinction was accompanied
537 by the presence of the genes *nirT* and *nirB* in the clade 1b NirS cluster, but not in the clade 1a cluster (Table
538 1). The *nirT* and *nirB* genes encode tetraheme and diheme *c*-type cytochromes, respectively. NirT belongs
539 to the NapC/NirT family of cytochromes, which are characterized by their electron transfer capacity.
540 Beyond this role, NirT may also catalytically activate cytochrome cd_1, indicating that it could serve as an
541 essential activating partner for NirS (Zajicek et al. 2004). Notably, NirT was shown to be essential for
542 functional NO_2^- reduction in *S. perfectomarina* strain ZoBell (Jüngst et al. 1991; Härtig and Zumft 1999).
543 These two proteins form a functional heterodimer since fused NirTB are found in other bacteria such as
544 *Halomonas* sp. 2A, which has been implicated in nitrite accumulation in a saline bioreactor (Li et al. 2018).
545 The involvement of the product of this gene in NO_2^- reduction is supported by its location immediately
546 downstream of *nirS*. Despite these indications of function, the extent to which NirT and NirB contribute to
547 the near-complete inhibition of NirS activity by NO_3^- in FNA strains remains unresolved. Our experiment
548 in which TMPD and ascorbate were added (Figure 5d-e) to provide excess electrons to NirS via cytochrome
549 c resulted in only a small reduction in NO_2^- accumulation, suggesting that NO_3^- inhibition of NirS in FNA
550 strains may involve a more direct interaction with NO_3^- through an as-yet unknown mechanism. In contrast
551 to the FNA phenotype, the LNA strain JM300 (Figure 5c) showed no disruption in NO_2^- reduction upon
552 NO_3^- addition, indicating a balanced electron distribution between NO_3^- and NO_2^- reduction.

553 One factor that may potentially have a role in NO_2^- accumulation is the FNR/CRP-related protein
554 DnrE, encoded by the gene *dnrE*, which is part of the *nar* cluster (Härtig et al. 1999). DnrE is considered
555 to play a role in the transcriptional regulation of *narG* in *Stutzerimonas sp.* (former *Pseudomonas stutzeri*).
556 The precise mechanism of DnrE control has not been elucidated, but it was reported that transcription levels
557 of *dnrE* peaked when both NO_3^- and O_2 are present (Härtig et al. 1999; Vollack et al. 1999). This suggests
558 that DnrE possibly regulates the expression of the *nar* operon during the transition from aerobic to anaerobic

559 respiration, triggering *narG* transcription when NO_3^- is present and O_2 is close to depletion. In our survey
560 we found that the *dnrE* gene was present in all strains of the FNA and PNA groups but absent in all LNA
561 strains (Table 1), making it a candidate gene for involvement in NO_2^- accumulation. We hypothesized that
562 knocking out *dnrE* would decrease or delay the transcription of *narG*, thereby slowing NO_3^- reduction and
563 reducing NO_2^- accumulation. To test this, we used the PNA strain 19SMN4, as we had a CRISPR-Cas9
564 system adapted to this organism. Contrary to our expectations, the deletion mutant showed enhanced
565 accumulation of NO_2^- (Figure 4), excluding DnrE from playing a direct regulatory role in causing NO_2^-
566 accumulation. It might, however, play a role in a more complex multilayered and interwoven regulation
567 mechanism (Spiro 2007; Spiro 2012).

568 In our search for additional regulatory mechanisms influencing denitrification, we examined the
569 potential role of small RNAs (sRNAs) in modulating NO_2^- accumulation in the FNA strain *S.*
570 *perfectomarina* ZoBell. Candidate sRNAs were selected based on their conservation across *Pseudomonas*
571 species, their genomic proximity to denitrification gene clusters, and previous associations with nitrogen
572 metabolism. Although several candidates were successfully overexpressed under anaerobic conditions, no
573 significant changes in NO_2^- accumulation were observed, suggesting that none of the selected sRNAs
574 directly regulates denitrification under the tested conditions although mutational analyses would be needed
575 to fully rule them out. These findings highlight the limitations of a candidate-based approach and emphasize
576 the need for broader transcriptomic analyses. In particular, *de novo* RNA-seq analyses, comparing closely
577 related *Stutzerimona*s strains exhibiting different NO_2^- accumulation phenotypes, could provide valuable
578 insight into the denitrification specific transcriptional landscape.

579 Conclusions

580 Our study demonstrated a large variation in denitrification phenotypes among closely related
581 *Stutzerimonas* strains, and revealed a complex interplay of genetic, transcriptional, and post-transcriptional
582 mechanisms influencing their NO_2^- accumulation. Organisms with a complete set of denitrification genes
583 can function as partial denitrifiers by transiently blocking specific steps in the process, as observed in the

584 FNA strains in our study. Avoiding or delaying the production of a complete denitrification proteome likely
585 conserves energy and may be advantageous in environments with fluctuating O_2 levels, where organisms
586 only need to rely on NO_3^- respiration for short periods. In the same way as "partial denitrifiers" lacking one
587 or more of the denitrification genes "share labour" (Roothans et al. 2025), FNA-like organisms depend on
588 community members that express the full denitrification proteome to maintain NO_2^- concentrations at non-
589 toxic levels. This prevents the accumulation of NO_2^- or the formation of harmful compounds like NO or
590 N_2O, including those arising from abiotic NO_2^- reactions (Lim et al. 2018). While the presence and timing
591 of *narG* transcription emerged as key factors, additional contributors, such as the type of *nirS* and
592 associated *nirT*/*nirB* genes, as well as competition for electrons between Nar and Nir pathways, were also
593 implicated. The results underscore the limitations of inferring NO_2^- accumulation potential based solely on
594 taxonomy or gene presence. These insights emphasize the multifaceted nature of denitrification regulation
595 and the need for more integrative approaches combining microbial physiology, biochemistry and
596 transcriptomics to further unravel mechanisms governing NO_2^- accumulation. Understanding these
597 processes is crucial for mitigating the environmental impacts of NO_2^- and related intermediate compounds,
598 particularly in contexts such as wastewater treatment and greenhouse gas emissions.
599

600 **Author contributions**

601 **Martin Menestreau:** investigations, formal analysis, visualization, data interpretation, writing – original
602 draft, writing – review and editing. **Daniel A. Milligan:** preliminary investigations (gas kinetics,
603 transcription, genome analyses), writing – early draft. **Louise B. Sennett:** data analysis (statistics), writing-
604 - editing. **Linda Bergaust:** data interpretation, writing – review and editing. **Lars R. Bakken** data
605 interpretation, writing – review and editing. **Gary Rowley:** supervision of sRNA work, writing – review
606 and editing. **Morten Kjos:** supervision of CRISPR analyses, writing – review and editing. **James P.**
607 **Shapleigh:** data analysis (phylogeny), data interpretation, validation, writing – review and editing. **Åsa**
608 **Frostegård:** conceptualization, funding acquisition, supervision, project administration, data

interpretation, validation, writing – original draft, writing – review and editing. All authors contributed to the article and approved the submitted version.

Acknowledgements

This work was supported by the Research Council of Norway, project no. 325770 (awarded to Å.F.).

Conflicts of interest

The authors declare no conflicts of interest

Data availability statement

The gas kinetics and transcription data that support the findings of this study are available on request from the corresponding author.

References

Aziz, R. K., Bartels, D., Best, A. A., DeJongh, M., Disz, T., Edwards, R. A., Formsma, K., Gerdes, S., Glass, E. M., Kubal, M., Meyer, F., Olsen, G. J., Olson, R., Osterman, A. L., Overbeek, R. A., McNeil, L. K., Paarmann, D., Paczian, T., Parrello, B., … Zagnitko, O. (2008). The RAST Server: Rapid Annotations using Subsystems Technology. *BMC Genomics*, *9*(1), 75. https://doi.org/10.1186/1471-2164-9-75

Bakken, L. R., Bergaust, L., Liu, B., & Frostegård, Å. (2012). Regulation of denitrification at the cellular level: A clue to the understanding of N_2O emissions from soils. *Philosophical Transactions of the Royal Society B: Biological Sciences*, *367*(1593), 1226–1234. https://doi.org/10.1098/rstb.2011.0321

Bergaust, L., Mao, Y., Bakken, L. R., & Frostegård, Å. (2010). Denitrification Response Patterns during the Transition to Anoxic Respiration and Posttranscriptional Effects of Suboptimal pH on Nitrogen Oxide Reductase in *Paracoccus denitrificans*. *Applied and Environmental Microbiology*, *76*(19), 6387–6396. https://doi.org/10.1128/AEM.00608-10

Bhattarai, H. R., Virkajärvi, P., Yli-Pirilä, P., & Maljanen, M. (2018). Emissions of atmospherically important nitrous acid (HONO) gas from northern grassland soil increases in the presence of nitrite (NO2−). *Agriculture, Ecosystems & Environment*, *256*, 194–199. https://doi.org/10.1016/j.agee.2018.01.017

Bollag, J.-M., & Henninger, N. M. (1978). Effects of nitrite toxicity on soil bacteria under aerobic and anaerobic conditions. *Soil Biology and Biochemistry*, *10*(5), 377–381. https://doi.org/10.1016/0038-0717(78)90061-5

Braman, R. S., & Hendrix, S. A. (1989). Nanogram nitrite and nitrate determination in environmental and biological materials by vanadium(III) reduction with chemiluminescence detection. *Analytical Chemistry*, *61*(24), 2715–2718. https://doi.org/10.1021/ac00199a007

Carlson, C. A., & Ingraham, J. L. (1983). Comparison of denitrification by Pseudomonas stutzeri, Pseudomonas aeruginosa, and Paracoccus denitrificans. *Applied and Environmental Microbiology*, *45*(4), 1247–1253. https://doi.org/10.1128/aem.45.4.1247-1253.1983

Chen, J., & Strous, M. (2013). Denitrification and aerobic respiration, hybrid electron transport chains and co-evolution. *Biochimica et Biophysica Acta (BBA) - Bioenergetics*, *1827*(2), 136–144. https://doi.org/10.1016/j.bbabio.2012.10.002

Chen, W., Zhang, Y., Zhang, Y., Pi, Y., Gu, T., Song, L., Wang, Y., & Ji, Q. (2018). CRISPR/Cas9-based Genome Editing in Pseudomonas aeruginosa and Cytidine Deaminase-Mediated Base Editing in Pseudomonas Species. *iScience*, *6*, 222–231. https://doi.org/10.1016/j.isci.2018.07.024

Choi, K.-H., Kumar, A., & Schweizer, H. P. (2006). A 10-min method for preparation of highly electrocompetent Pseudomonas aeruginosa cells: Application for DNA fragment transfer between chromosomes and plasmid transformation. *Journal of Microbiological Methods*, *64*(3), 391–397. https://doi.org/10.1016/j.mimet.2005.06.001

Cole. (2025). Nitrate reduction for survival in a nanomolar world, not the millimolar world of a laboratory. In Advances in Microbial Physiology (Vol. 87, pp. 79–117). Elsevier. https://doi.org/10.1016/bs.ampbs.2025.07.005

Concordet, J.-P., & Haeussler, M. (2018). CRISPOR: Intuitive guide selection for CRISPR/Cas9 genome editing experiments and screens. *Nucleic Acids Research*, *46*(W1), W242–W245. https://doi.org/10.1093/nar/gky354

Cox, R. D. (1980). Determination of nitrate and nitrite at the parts per billion level by chemiluminescence. *Analytical Chemistry*, *52*(2), 332–335. https://doi.org/10.1021/ac50052a028

Decleyre, H., Tytgat, B., & Anne, W. (2016). Highly diverse nirK genes comprise two major clades that harbour ammonium-producing denitrifiers. *BMC Genomics*, *17*(1), 155. https://doi.org/10.1186/s12864-016-2465-0

Ebert, M., Laaß, S., Thürmer, A., Roselius, L., Eckweiler, D., Daniel, R., Härtig, E., & Jahn, D. (2017). FnrL and three Dnr regulators are used for the metabolic adaptation to low oxygen tension in *Dinoroseobacter shibae*. *Frontiers in Microbiology*, *8*, 642. https://doi.org/10.3389/fmicb.2017.00642

Edgar, R. C. (2004). MUSCLE: Multiple sequence alignment with high accuracy and high throughput. *Nucleic Acids Research*, *32*(5), 1792–1797. https://doi.org/10.1093/nar/gkh340

Frostegård, Å., Vick, S. H. W., Lim, N. Y. N., Bakken, L. R., & Shapleigh, J. P. (2022). Linking meta-omics to the kinetics of denitrification intermediates reveals pH-dependent causes of N2O emissions and nitrite accumulation in soil. *The ISME Journal*, *16*(1), 26–37. https://doi.org/10.1038/s41396-021-01045-2

Gaimster, H., Alston, M., Richardson, D. J., Gates, A. J., & Rowley, G. (2018). Transcriptional and environmental control of bacterial denitrification and N2O emissions. *FEMS Microbiology Letters*, *365*(5). https://doi.org/10.1093/femsle/fnx277

Gaimster, H., Hews, C. L., Griffiths, R., Soriano-Laguna, M. J., Alston, M., Richardson, D. J., Gates, A. J., & Rowley, G. (2019). A central small RNA regulatory circuit controlling bacterial denitrification and N_2 O emissions. *mBio*, *10*(4), e01165-19. https://doi.org/10.1128/mBio.01165-19

Gao, Y., Mania, D., Mousavi, S. A., Lycus, P., Arntzen, M. Ø., Woliy, K., Lindström, K., Shapleigh, J. P., Bakken, L. R., & Frostegård, Å. (2021). Competition for electrons favours N_2 O reduction in denitrifying *Bradyrhizobium* isolates. *Environmental Microbiology*, *23*(4), 2244–2259. https://doi.org/10.1111/1462-2920.15404

682 Gomila, M., Mulet, M., García-Valdés, E., & Lalucat, J. (2022). Genome-Based Taxonomy of the Genus
683 Stutzerimonas and Proposal of S. frequens sp. Nov. And S. degradans sp. Nov. And Emended Descriptions
684 of S. perfectomarina and S. chloritidismutans. *Microorganisms*, *10*(7), 1363.
685 https://doi.org/10.3390/microorganisms10071363

686 Guindon, S., Dufayard, J.-F., Lefort, V., Anisimova, M., Hordijk, W., & Gascuel, O. (2010). New algorithms
687 and methods to estimate maximum-likelihood phylogenies: Assessing the performance of PhyML 3.0.
688 *Systematic Biology*, *59*(3), 307–321. https://doi.org/10.1093/sysbio/syq010

689 Härtig, E., Schiek, U., Vollack, K.-U., & Zumft, W. G. (1999). Nitrate and Nitrite Control of Respiratory
690 Nitrate Reduction in Denitrifying *Pseudomonas stutzeri* by a Two-Component Regulatory System
691 Homologous to NarXL of *Escherichia coli*. *Journal of Bacteriology*, *181*(12), 3658–3665.
692 https://doi.org/10.1128/JB.181.12.3658-3665.1999

693 Härtig, E., & Zumft, W. G. (1999). Kinetics of *nirS* Expression (Cytochrome cd_1 Nitrite Reductase) in
694 *Pseudomonas stutzeri* during the Transition from Aerobic Respiration to Denitrification: Evidence for a
695 Denitrification-Specific Nitrate- and Nitrite-Responsive Regulatory System. *Journal of Bacteriology*,
696 *181*(1), 161–166. https://doi.org/10.1128/JB.181.1.161-166.1999

697 Heider, J., & Fuchs, G. (2015). *Thauera*. In W. B. Whitman (Ed.), *Bergey's Manual of Systematics of*
698 *Archaea and Bacteria* (1st ed., pp. 1–11). Wiley. https://doi.org/10.1002/9781118960608.gbm01004

699 Ingram. (1973). *The microbiological effects of nitrite*. In International Symposium of Nitrite in Meat
700 Products. Zeist. Netherlands (B. Krol and B. J. Tinbergen, Eds). pp. 63-75. Wageningen, Pudoc, 1974.

701 Jones, C. M., Stres, B., Rosenquist, M., & Hallin, S. (2008). Phylogenetic Analysis of Nitrite, Nitric Oxide,
702 and Nitrous Oxide Respiratory Enzymes Reveal a Complex Evolutionary History for Denitrification.
703 *Molecular Biology and Evolution*, *25*(9), 1955–1966. https://doi.org/10.1093/molbev/msn146

704 Jüngst, A., Wakabayashi, S., Matsubara, H., & Zumft, W. G. (1991). The *nirSTBM* region coding for
705 cytochrome cd_1 -dependent nitrite respiration of *Pseudomonas stutzeri* consists of a cluster of mono-, di-,
706 and tetraheme proteins. *FEBS Letters*, *279*(2), 205–209. https://doi.org/10.1016/0014-5793(91)80150-2

707 Kuypers, M. M. M., Marchant, H. K., & Kartal, B. (2018). The microbial nitrogen-cycling network. *Nature*
708 *Reviews Microbiology*, *16*(5), 263–276. https://doi.org/10.1038/nrmicro.2018.9

709 Lalucat, J., Bennasar, A., Bosch, R., García-Valdés, E., & Palleroni, N. J. (2006). Biology of *Pseudomonas*
710 *stutzeri*. *Microbiology and Molecular Biology Reviews*, *70*(2), 510–547.
711 https://doi.org/10.1128/MMBR.00047-05

712 Lalucat, J., Gomila, M., Mulet, M., Zaruma, A., & García-Valdés, E. (2022). Past, present and future of the
713 boundaries of the Pseudomonas genus: Proposal of Stutzerimonas gen. Nov. *Systematic and Applied*
714 *Microbiology*, *45*(1), 126289. https://doi.org/10.1016/j.syapm.2021.126289

715 Li, W., Li, H., Liu, Y., Zheng, P., & Shapleigh, J. P. (2018). Salinity-Aided Selection of Progressive Onset
716 Denitrifiers as a Means of Providing Nitrite for Anammox. *Environmental Science & Technology*, *52*(18),
717 10665–10672. https://doi.org/10.1021/acs.est.8b02314

718 Li, X., Yang, Z., Wang, Z., Li, W., Zhang, G., & Yan, H. (2022). Comparative Genomics of Pseudomonas
719 stutzeri Complex: Taxonomic Assignments and Genetic Diversity. *Frontiers in Microbiology*, *12*, 755874.
720 https://doi.org/10.3389/fmicb.2021.755874

Lim, N. Y. N., Frostegård, Å., & Bakken, L. R. (2018). Nitrite kinetics during anoxia: The role of abiotic reactions versus microbial reduction. *Soil Biology and Biochemistry*, *119*, 203–209. https://doi.org/10.1016/j.soilbio.2018.01.006

Lim, N. Y. N., Roco, C. A., & Frostegård, Å. (2016). Transparent DNA/RNA Co-extraction Workflow Protocol Suitable for Inhibitor-Rich Environmental Samples That Focuses on Complete DNA Removal for Transcriptomic Analyses. *Frontiers in Microbiology*, *7*. https://doi.org/10.3389/fmicb.2016.01588

Lin, M., Yan, Y., Lu, W., Zhan, Y., Zhang, Y., & Elmerich, C. (2015). Regulatory Coupling of Nitrogen and Carbon Metabolism in Nitrogen-Fixing *Pseudomonas stutzeri* A1501. In F. J. De Bruijn (Ed.), *Biological Nitrogen Fixation* (1st ed., pp. 109–120). Wiley. https://doi.org/10.1002/9781119053095.ch10

Liu, B., Mao, Y., Bergaust, L., Bakken, L. R., & Frostegård, Å. (2013). Strains in the genus *Thauera* exhibit remarkably different denitrification regulatory phenotypes. *Environmental Microbiology*, *15*(10), 2816–2828. https://doi.org/10.1111/1462-2920.12142

Lycus, P., Lovise Bøthun, K., Bergaust, L., Peele Shapleigh, J., Reier Bakken, L., & Frostegård, Å. (2017). Phenotypic and genotypic richness of denitrifiers revealed by a novel isolation strategy. *The ISME Journal*, *11*(10), 2219–2232. https://doi.org/10.1038/ismej.2017.82

Lycus, P., Soriano-Laguna, M. J., Kjos, M., Richardson, D. J., Gates, A. J., Milligan, D. A., Frostegård, Å., Bergaust, L., & Bakken, L. R. (2018). A bet-hedging strategy for denitrifying bacteria curtails their release of N_2 O. *Proceedings of the National Academy of Sciences*, *115*(46), 11820–11825. https://doi.org/10.1073/pnas.1805000115

Mania, D., Woliy, K., Degefu, T., & Frostegård, Å. (2020). A common mechanism for efficient N_2 O reduction in diverse isolates of nodule-forming bradyrhizobia. *Environmental Microbiology*, *22*(1), 17–31. https://doi.org/10.1111/1462-2920.14731

Massé, E., & Gottesman, S. (2002). A small RNA regulates the expression of genes involved in iron metabolism in *Escherichia coli*. *Proceedings of the National Academy of Sciences*, *99*(7), 4620–4625. https://doi.org/10.1073/pnas.032066599

Moeller, S., Payá, G., Bonete, M.-J., Gates, A. J., Richardson, D. J., Esclapez, J., & Rowley, G. (2021). Microbial Small RNAs – The Missing Link in the Nitrogen Cycle? *Frontiers in Environmental Science*, *9*, 660055. https://doi.org/10.3389/fenvs.2021.660055

Molstad, L., Dörsch, P., & Bakken, L. R. (2007). Robotized incubation system for monitoring gases (O2, NO, N2O N2) in denitrifying cultures. *Journal of Microbiological Methods*, *71*(3), 202–211. https://doi.org/10.1016/j.mimet.2007.08.011

Molstad, L., Dörsch, P., & Bakken, L. R. (2016). *Improved robotized incubation system for gas kinetics in batch cultures*. Unpublished. https://doi.org/10.13140/RG.2.2.30688.07680

Philippot, L. (2002). Denitrifying genes in bacterial and Archaeal genomes. *Biochimica et Biophysica Acta (BBA) - Gene Structure and Expression*, *1577*(3), 355–376. https://doi.org/10.1016/S0167-4781(02)00420-7

Pold, G., Bonilla-Rosso, G., Saghaï, A., Strous, M., Jones, C. M., & Hallin, S. (2024). Phylogenetics and environmental distribution of nitric oxide-forming nitrite reductases reveal their distinct functional and ecological roles. *ISME Communications*, *4*(1), ycae020. https://doi.org/10.1093/ismeco/ycae020

Richarson, D. (2025). Life on oxidised nitrogen: The biochemistry and physiology of prokaryotic life supported by the nitrate-nitrite redox couple. In *Advances in Microbial Physiology* (Vol. 87, pp. 11–77). Elsevier. https://doi.org/10.1016/bs.ampbs.2025.07.004

Roothans, N., Van Loosdrecht, M. C. M., & Laureni, M. (2025). Metabolic labour division trade-offs in denitrifying microbiomes. *The ISME Journal*, *19*(1), wraf020. https://doi.org/10.1093/ismejo/wraf020

Shapleigh, J. P. (2013). Denitrifying Prokaryotes. In E. Rosenberg, E. F. DeLong, S. Lory, E. Stackebrandt, & F. Thompson (Eds.), *The Prokaryotes* (pp. 405–425). Springer Berlin Heidelberg. https://doi.org/10.1007/978-3-642-30141-4_71

Sievers, F., Wilm, A., Dineen, D., Gibson, T. J., Karplus, K., Li, W., Lopez, R., McWilliam, H., Remmert, M., Söding, J., Thompson, J. D., & Higgins, D. G. (2011). Fast, scalable generation of high-quality protein multiple sequence alignments using Clustal Omega. *Molecular Systems Biology*, *7*(1), 539. https://doi.org/10.1038/msb.2011.75

Sistrom, W. R. (1960). A Requirement for Sodium in the Growth of Rhodopseudomonas spheroides. *Journal of General Microbiology*, *22*(3), 778–785. https://doi.org/10.1099/00221287-22-3-778

Sommer, M., Xie, H., & Michel, H. (2017). Pseudomonas stutzeri as an alternative host for membrane proteins. *Microbial Cell Factories*, *16*(1), 157. https://doi.org/10.1186/s12934-017-0771-0

Song, M., Zhao, X., Liu, P., Mu, J., He, G., Zhang, C., Tong, S., Xue, C., Zhao, X., Ge, M., & Mu, Y. (2023). Atmospheric NOx oxidation as major sources for nitrous acid (HONO). *Npj Climate and Atmospheric Science*, *6*(1), 30. https://doi.org/10.1038/s41612-023-00357-8

Spiro, S. (2007). Regulators of bacterial responses to nitric oxide. *FEMS Microbiology Reviews*, *31*(2), 193–211. https://doi.org/10.1111/j.1574-6976.2006.00061.x

Spiro, S. (2012). Nitrous oxide production and consumption: Regulation of gene expression by gas-sensitive transcription factors. *Philosophical Transactions of the Royal Society B: Biological Sciences*, *367*(1593), 1213–1225. https://doi.org/10.1098/rstb.2011.0309

Trunk, K., Benkert, B., Quäck, N., Münch, R., Scheer, M., Garbe, J., Jänsch, L., Trost, M., Wehland, J., Buer, J., Jahn, M., Schobert, M., & Jahn, D. (2010). Anaerobic adaptation in *Pseudomonas aeruginosa*: Definition of the Anr and Dnr regulons. *Environmental Microbiology*, *12*(6), 1719–1733. https://doi.org/10.1111/j.1462-2920.2010.02252.x

Vaccaro, B. J., Thorgersen, M. P., Lancaster, W. A., Price, M. N., Wetmore, K. M., Poole, F. L., Deutschbauer, A., Arkin, A. P., & Adams, M. W. W. (2016). Determining Roles of Accessory Genes in Denitrification by Mutant Fitness Analyses. *Applied and Environmental Microbiology*, *82*(1), 51–61. https://doi.org/10.1128/AEM.02602-15

Van Cleemput, O., & Samater, A. H. (1995). Nitrite in soils: Accumulation and role in the formation of gaseous N compounds. *Fertilizer Research*, *45*(1), 81–89. https://doi.org/10.1007/BF00749884

Vollack, K., Härtig, E., Körner, H., & Zumft, W. G. (1999). Multiple transcription factors of the FNR family in denitrifying *Pseudomonas stutzeri*: Characterization of four *fnr* -like genes, regulatory responses and cognate metabolic processes. *Molecular Microbiology*, *31*(6), 1681–1694. https://doi.org/10.1046/j.1365-2958.1999.01302.x

Vollack, K.-U., Xie, J., Härtig, E., Römling, U., & Zumft, W. G. (1998). Localization of denitrification genes on the chromosomal map of Pseudomonas aeruginosa. *Microbiology*, *144*(2), 441–448. https://doi.org/10.1099/00221287-144-2-441

Wang, M., Liang, Y., Li, F., Shen, S., Huang, X., & Sun, Y. (2022). Enhancement of biological denitrification by the addition of novel sRNA Pda200 under antibiotic pressure. *Bioresource Technology*, *365*, 128113. https://doi.org/10.1016/j.biortech.2022.128113

Wittorf, L., Jones, C. M., Bonilla-Rosso, G., & Hallin, S. (2018). Expression of nirK and nirS genes in two strains of Pseudomonas stutzeri harbouring both types of NO-forming nitrite reductases. *Research in Microbiology*, *169*(6), 343–347. https://doi.org/10.1016/j.resmic.2018.04.010

Zajicek, R. S., Allen, J. W. A., Cartron, M. L., Richardson, D. J., & Ferguson, S. J. (2004). *Paracoccus pantotrophus* NapC can reductively activate cytochrome cd_1 nitrite reductase. *FEBS Letters*, *565*(1–3), 48–52. https://doi.org/10.1016/j.febslet.2004.03.072

Zerbino, D. R., & Birney, E. (2008). Velvet: Algorithms for de novo short read assembly using de Bruijn graphs. *Genome Research*, *18*(5), 821–829. https://doi.org/10.1101/gr.074492.107

Zhan, Y., Yan, Y., Deng, Z., Chen, M., Lu, W., Lu, C., Shang, L., Yang, Z., Zhang, W., Wang, W., Li, Y., Ke, Q., Lu, J., Xu, Y., Zhang, L., Xie, Z., Cheng, Q., Elmerich, C., & Lin, M. (2016). The novel regulatory ncRNA, NfiS, optimizes nitrogen fixation via base pairing with the nitrogenase gene *nifK* mRNA in *Pseudomonas stutzeri* A1501. *Proceedings of the National Academy of Sciences*, *113*(30). https://doi.org/10.1073/pnas.1604514113

Zhou, Y., Oehmen, A., Lim, M., Vadivelu, V., & Ng, W. J. (2011). The role of nitrite and free nitrous acid (FNA) in wastewater treatment plants. *Water Research*, *45*(15), 4672–4682. https://doi.org/10.1016/j.watres.2011.06.025

Zhuang, J.-L., Sun, X., Zhao, W.-Q., Zhang, X., Zhou, J.-J., Ni, B.-J., Liu, Y.-D., Shapleigh, J. P., & Li, W. (2022). The anammox coupled partial-denitrification process in an integrated granular sludge and fixed-biofilm reactor developed for mainstream wastewater treatment: Performance and community structure. *Water Research*, *210*, 117964. https://doi.org/10.1016/j.watres.2021.117964

ZoBell, C. E., & Upham, H. C. (1944). *A List of Marine Bacteria Including Descriptions of Sixty New Species*. University of California Press. https://books.google.no/books?id=mijZAAAAMAAJ

Zumft, W. G. (1997). Cell biology and molecular basis of denitrification. *Microbiology and Molecular Biology Reviews*, *61*(4), 533–616. https://doi.org/10.1128/mmbr.61.4.533-616.1997

		NO_3^- to NO_2^-			NO_2^- to NO				NO to N_2O	N_2O to N_2	Maximum Denitrification intermediates accumulation (NO_2^- µmol vial^{-1}, NO and N_2O nmol vial^{-1})						
		Periplasmic nitrate red.	Membrane-bound nitrate red.		Cytochrome cd_1-nitrite red.			Copper nitrite red.	c-Nitric oxide red.	Nitrous oxide red. clade I							
Group	Strain	*napABCDE*	*narGHJIKMXL*	*dnrE*	NirS clade	*nirJENY*	*nirTB*	NirK clade	*norBCD*	*nosRZDFYL*	Max NO_2^-		Max NO		Max N_2O		
FNA	CCUG 36651	+	+	+	Clade 1b	downstream	+	clade II	+	+	96.5 ± 0.6	a	39.3 ± 0.3	abc	22.1 ± 1.0	a	
	DSM 50227	+	+	+	Clade 1b	downstream	+	clade II	+	+	101.4 ± 5.7		62.5 ± 15.5		7.7 ± 1.7		
	ATCC 17591	+	+	+	Clade 1b	downstream	+	clade II	+	+	92.9 ± 0.4		26.5 ± 4.2		15.8 ± 2.2		
	ZoBell	+	+	+	Clade 1b	downstream	+	–	+	+	108.8 ± 0.25		70.5 ± 5.0		11.8 ± 1.2		
	24a13	+	+	+	Clade 1b	downstream	+	clade II	+	+	71.7 ± 5.7		32.1 ± 2.8		19.7 ± 1.3		
	KC	+	+	+	Clade 1b	downstream	+	–	+	+	96.7 ± 0.2		25.0 ± 0.6		13.7 ± 0.2		
	ST27MN3	+	+	+	Clade 1b	downstream	+	–	+	+	101.5 ± 6.0		20.1 ± 3.4		0.3 ± 0.1		
	CMT.9.A	+	+	+	Clade 1b	downstream	+	–	+	+	89.1 ± 1.6		27.5 ± 2.7		16.1 ± 1.4		
PNA	AN10	+	+	+	Clade 1a	downstream	–	clade II	+	+	62.2 ± 4.8	b	25.6 ± 5.0	abc	24.9 ± 1.8	ab	
	19SMN4	+	+	+	Clade 1a	downstream	–	–	+	+	44.0 ± 2.5		29.3 ± 1.7		25.6 ± 3.0		
	CCUG 11256	+	+	+	Clade 1a	downstream	–	–	+	+	43.7 ± 3.3		20.4 ± 1.6		18.0 ± 1.2		
LNA	DNSP21	+	–	–	Clade 1a	downstream	–	–	+	+	1.2 ± 0.01	c	9.1 ± 0.6	abc	6.5 ± 0.3	bc	
	24a75	+	+	–	Clade 1a	downstream	–	–	+	+	11.3 ± 0.7		47.4 ± 4.3		83.7 ± 44.6		
	DSM 50238	+	+	–	Clade 1a	downstream	–	–	+	+	0.01 ± 0.01		13.9 ± 0.7		56.9 ± 13.6		
	DSM 18231	+	+	–	Clade 1a	upstream	–	clade I	+	+	0.2 ± 0.07		43.1 ± 4.2		21.4 ± 5.6		
	4C29	+	+	–	Clade 1a	upstream	–	–	+	+	17.1 ± 6.7		41.2 ± 3.0		88.9 ± 26.5		
	28a3	+	–	–	Clade 1a	upstream	–	–	+	+	1.38 ± 0.01		28.4 ± 8.5		52.6 ± 27.5		
	JM300	+	+	–	Clade 1b	upstream	+	clade I	+	+	1.6 ± 0.04		38.6 ± 13.8		67.0 ± 25.7		

Table 1. Denitrification-related genetic features and maximum accumulation of the intermediate products of 18 *Stutzerimonas* strains. The strains were characterized and grouped as full nitrite accumulators (FNA), partial nitrite accumulators (PNA) or low nitrite accumulators (LNA). The two nitrite reductases NirS and NirK were classified into different clades according to Jones et al. (2008). The genetic organization of the *nirS* related clusters *nirMCFDLGH*, located directly downstream and *nirQOP,* positioned directly upstream of *nirS*, was the same in all strains. These are therefore not mentioned in the table. The *nirJENY* cluster was found either upstream or downstream of *nirS*, depending on the strain. All *nirK* clade I genes were accompanied by the accessory gene *nirV*, located directly downstream of the *nirK* gene, while all *nirK* clade II genes were followed by an extra *norCBQD* gene cluster, not shown in the table. Statistical significance for the maximum denitrification intermediates accumulation was assessed using one-way ANOVAs (p = 0.05). Post hoc multiple comparisons of means were conducted using Tukey´s Honest Significant Difference (HSD; p = 0.05) tests. Statistical differences are indicated where the groups sharing the same letter are not statistically different.

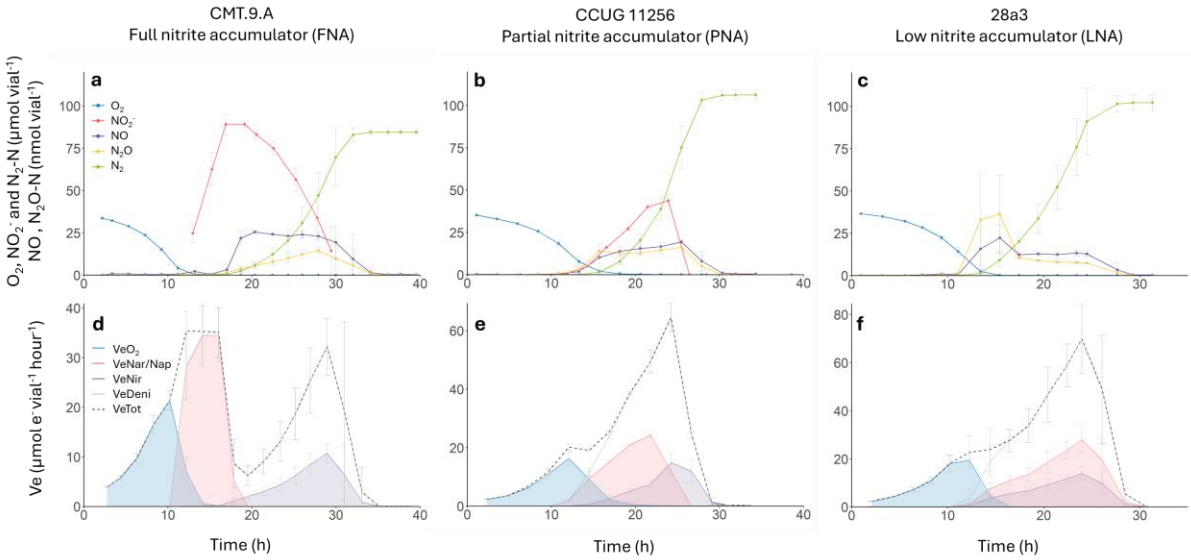

Figure 1. Denitrification kinetics (a–c) and electron flow rates to reductases (d–f) during and after the transition from aerobic respiration to denitrification. Strains were incubated at 20 °C in 120 mL medical vials containing 50 mL Sistrom's mineral medium, supplemented with KNO_3 to an initial concentration of 2 mM (100 µmol vial^{-1}), with He and 1% O_2 in the headspace. The panels show the results for three strains representing the FNA, PNA, and LNA groups. The upper panels show the measured NO_2^- and gases and the lower panels show the calculated rate of electron flow to O_2 (blue), NO_3^- (red), and NO_2^- (purple), with the total electron flow shown as a dashed line. All graphs show mean values from three independent replicates (n = 3); error bars represent standard deviation.

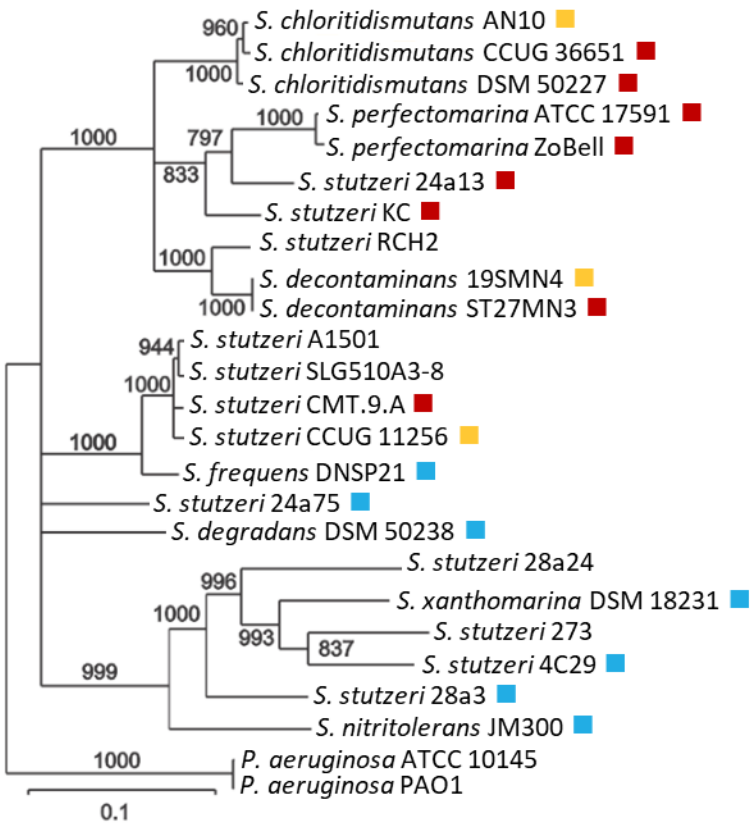

Figure 2. Maximum likelihood phylogenetic tree of selected *Stutzerimonas* strains and their NO_2^- accumulation phenotype. The three NO_2^- accumulation groups are indicated by different colors in the phylogenetic tree. Red: Full NO_2^- accumulators (FNA); reduced almost all available NO_3^- before reducing any NO_2^-. Yellow: Partial NO_2^- accumulators (PNA); transient accumulation of NO_2^- reaching approximately 40-60% of the amount of added NO_3^- Blue: Low NO_2^- accumulators (LNA); 0-20% of the reduced NO_3^- was transiently accumulated as NO_2^-. The phylogenetic analysis was a multilocus sequence analysis (MLSA) based on concatenated sequences of partial 16S rRNA and full *gyrB* and *rpoD* gene sequences. In addition to the strains analyzed for denitrification phenotypes, some other strains were included for which complete genome sequence data were publicly available. Only branches with bootstrap values ≥ 700 (of 1000) are shown. The strains were until recently included in a species complex encompassing the former *Pseudomonas stutzeri* and closely related strains (Li et al. 2022) but were recently circumscribed into several species of the novel genus *Stutzerimonas* (Laculat et al. 2022; Gomila et al. 2022). A list of the strains, including their origin and culture collection numbers, is provided in Table S1. A more detailed tree based on genome clustering, including all presently available *Stutzerimonas* genomes, is found in Figure S4.

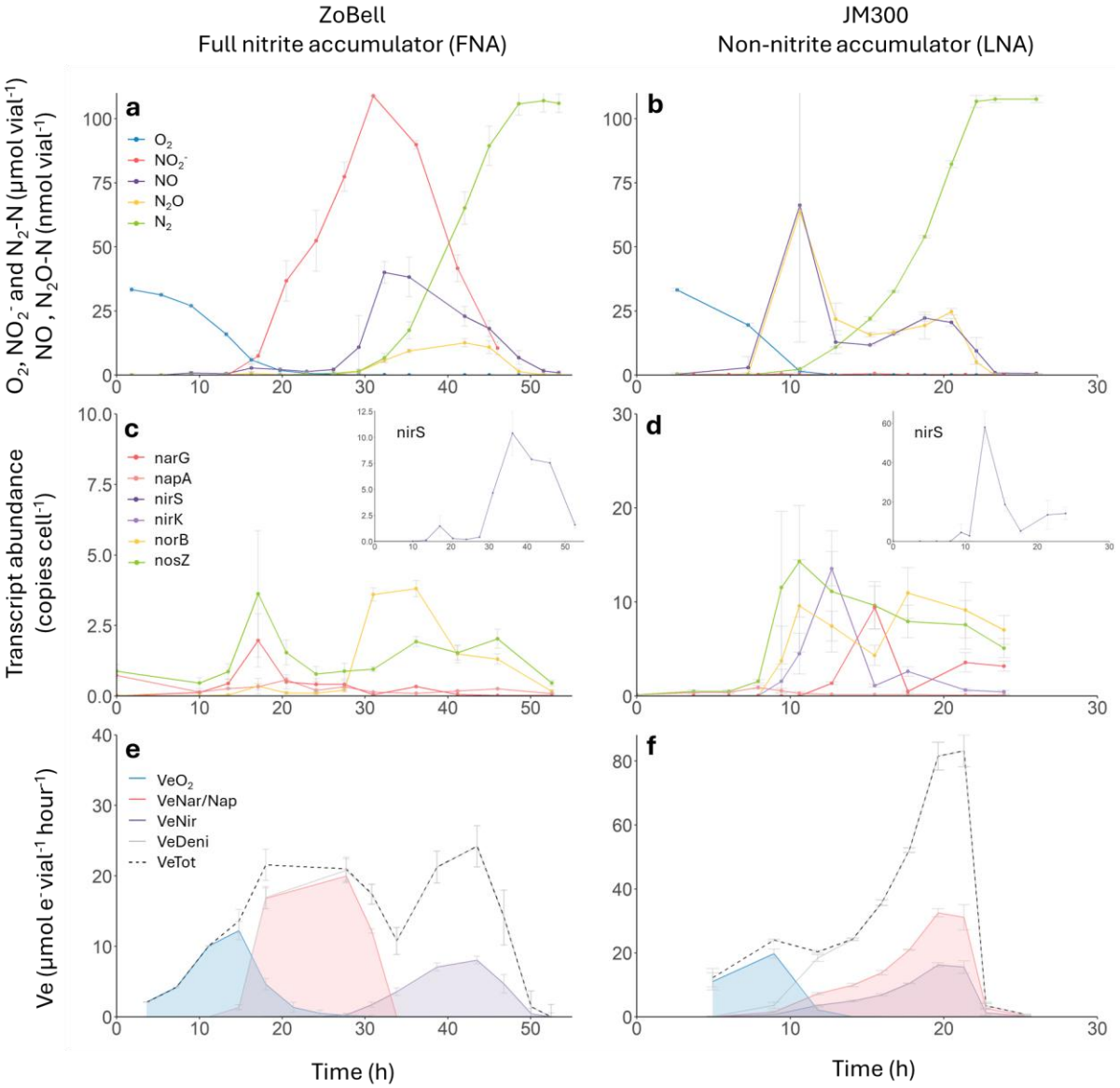

Figure 3. Denitrification kinetics, gene transcription and electron flow in the FNA strain ZoBell and the LNA strain JM300, switching from aerobic to anaerobic respiration. The panels show measured NO_2^- and gases (a, b), the denitrification gene transcription (c, d), and electron flow rates to reductases (e, f) during and after the transition from aerobic respiration to denitrification. Strains were incubated at 20 °C in 120 mL medical vials containing 50 mL Sistrom's mineral medium, supplemented with KNO_3 to an initial concentration of 2 mM (100 µmol vial^{-1}), with He and 1% O_2 in the headspace. Graphs show mean values from six independent replicates (n = 6); error bars represent standard deviation.

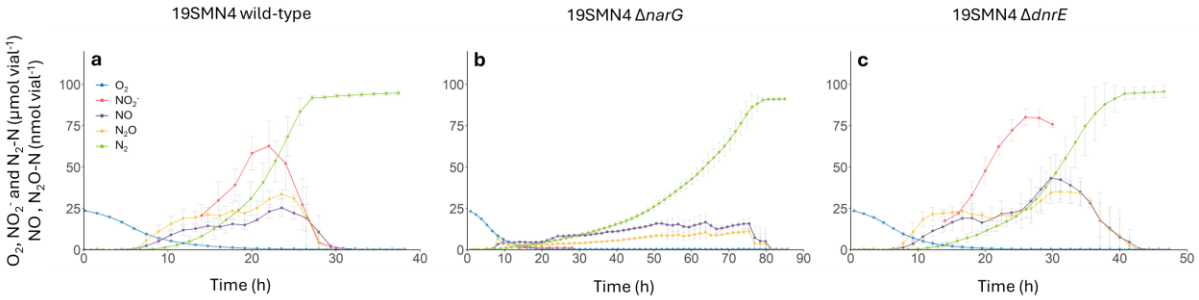

Figure 4. Effect of deleting *narG* and *dnrE* on the phenotype of the PNA strain *Stutzerimonas decontaminans* 19SMN4. The panels show the measured NO_2^- and gases during and after the transition from aerobic respiration to denitrification for the wild type (a), *narG* deletion mutant (b) and *dnrE* deletion mutant (c). Strains were incubated at 20 °C in 120 mL medical vials containing 50 mL Sistrom's mineral medium, supplemented with KNO_3 to an initial concentration of 2 mM (100 µmol vial^{-1}), with He and 1% O_2 in the headspace. Graphs show mean values from three independent replicates (n = 3); error bars represent standard deviation.

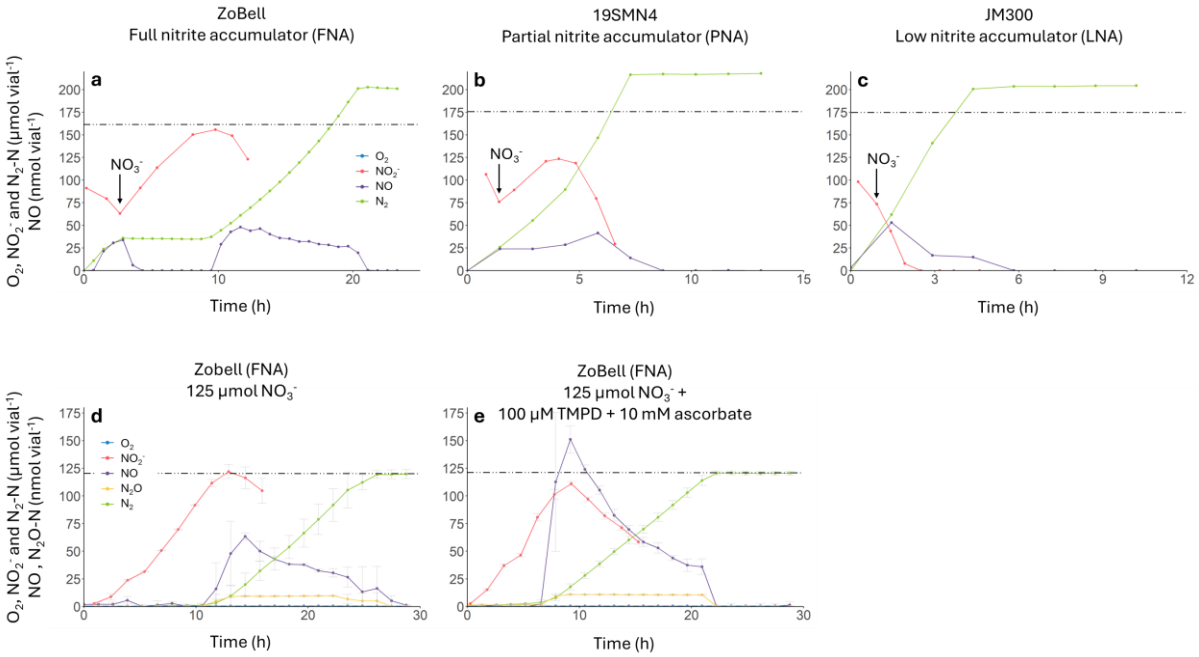

Figure 5. Competition for electrons between NO_3^- and NO_2^- reduction pathways. Results for three *Stutzerimonas* strains, each representing one of the three nitrite accumulation phenotypes (a–c). Experiments were performed in biological triplicates (n = 3). The timing of NO_3^- addition varied between replicate vials; therefore, one representative replicate is shown here, while the other replicates, which displayed very similar patterns, are presented in Fig. S7. Cultures were pre-grown anoxically (100% He headspace) in Sistrom's medium with NO_3^- to induce full denitrification proteomes, then transferred at t = 0 to fresh anoxic vials containing only 2 mM NO_2^- (100 µmol vial^{-1}). When approximately one-third of the NO_2^- was reduced, 100 µmol of NO_3^- (corresponding to 2 mM in the medium) was added (indicated by the arrow). Panels (d–e) show the effect of the artificial electron donor TMPD on an FNA strain. After similar pre-growth, the cells were supplied at t = 0 with 2.5 mM NO_3^- 125 µmol vial^{-1}), with (panel e) or without (panel d) 100 µM TMPD and 10 mM ascorbate. The dashed line represents the theoretical maximum NO_2^- accumulation. Graphs d and e show mean values from three independent replicates (n = 3); error bars represent standard deviation.